Segmentation, autofocusing and signature extraction of tuberculosis sputum images

Manuel Forero-Vargas[a],Filip Sroubek[d],Josue Alvarez-Borrego[c],
Norberto Malpica[b],Gabriel Cristóbal[c],Andrés Santos[b],Luis Alcala[f], Manuel Desco[f]
and Leon Cohen[g]

[a] Universidad Nacional de Colombia, Bogotá, Colombia
[b] ETS de Ingenieros de Telecomunicación, Ciudad Universitaria, Madrid, Spain
[c] División de Física Aplicada, División de Optica (CICESE), Ensenada, Mexico
[d] Institute of Information Theory and Automation, Prage, Czech Republic
[e] Instituto de Optica (CSIC), Serrano 121, Madrid, Spain
[f] Hospital Gregorio Marañón, Unidad de Medicina y Cirugía Experimental, Madrid, Spain
[g] Hunter College and Graduate Center of CUNY, NY 10021, USA

ABSTRACT

Bacteria segmentation of particular species entails a challenging process. Bacteria shape is not enough as a discriminant feature, because there are many species that share the same shape. We present here two methods for tuberculosis image segmentation using the chromatic information. The first method is based on fuzzy segmentation of the color images based on the information that it is entailed in each separate chromatic histogram. The second method is a simple color filtering account by comparison of the inverse of the yellowish stained bacteria (blue channel) with the product of the other two chromatic channels. The third method is based on the extraction of image signatures by projecting logarithmic-polar mappings onto 1D vectors. This representation provides a very compact description of all image aspects, including shape, texture and color. An achromatic segmentation method is also presented based on the use of gray-level morphological operators only to the green channel. Finally we present the results of different autofocusing algorithms of stained tuberculosis images.

Keywords: tuberculosis, fluorescence microscopy, feature detection, color, mass screening

1. INTRODUCTION

Several authors have addressed the segmentation of bacteria particles using different techniques. Veropoulos et al [1] used an identification method based on shape descriptors and neural network classifiers showing a sensitivity (the ratio of true positive decisions to the total number of positives) of 94.1 %. Wilkinson [2] has proposed a rapid multiresolution segmentation technique based on computing a different threshold for different areas of a grey-level image. Other authors have considered the use the color information as the key discriminant factor either for bacteria segmentation and identification [3,4] or for cell segmentation for lung cancer diagnosis [5,6]. Manual screening for the identification of bacilli involves a labor intensive task with a high false negative rate [1]. Automatic screening will entail several advantages, e.g. a substantial reduction in the labor workload of the clinicians and a better accuracy in diagnosis by increasing the number of images that can be analyzed by the computer. As a follow-up of the results described in,[7] in this paper we describe two basic techniques for bacteria segmentation based on the use of the chromatic information: a multi-thresholding image segmentation technique and a simple color filtering account by comparison of the inverse of the yellowish stained bacteria (blue channel) with the product of the other two chromatic channels. The second approach to segmentation is

Further author information: (Send correspondence to G.Cristobal: E-mail: gabriel@optica.csic.es; Tel: 34-91-561-6800; FAX: 34-91-564-5557)

based on the use of gray-level morphological operators only to the green channel. Objects are detected using mathematical morphology operators, and are then classified according to several shape and grey level features. Also, we describe an image identification method based on the use of the so-called *signatures*. The motivation for using signatures is to provide a representation invariant to rigid changes for improving the identification process but simultaneously reducing the dimensionality of the data. Finally, we present the results of different autofocusing methods of stained tuberculosis images.

2. MATERIALS AND METHODS

Staining procedures were performed with both respiratory and non-respiratory clinical specimens except for urine and blood specimens. These specimens were stained with the fluorochrome auramine O and were scanned at x250 magnifications with a fluorescence microscope. If present, the M. tuberculosis bacilli fluoresced yellow to green. Because acid-fast artifacts may be present in a smear, it is necessary to view cell morphology carefully. AFB are approximately 0.2 to 0.6 by 1 to 10 μm in size, curved or bent. Individual bacilli may display heavily stained areas and areas of alternating stain producing a beaded appearance. Confirmation of positive fluorochrome smears was made with the growth of M. tuberculosis bacilli from the culture of specimens in liquid and solid media. In such way, we can perform a region segmentation based on the RGB color image components. Sample slides were analyzed with a Zeiss Axiophot photomicroscope illuminated with a Zeiss Attoarc variable intensity fluorescence illumination system. For image acquisition we used a Coolsnap digital camera from Photometrics. Identification of tubercle bacilli are routinely done in sputum smears using a fluorescence microscope dyed with fluorochrome auramine.

3. CHROMATIC IMAGE SEGMENTATION

3.1. Multi-thresholding fuzzy segmentation

The concept of multi-thresholding for gray level segmentation can be extended for multichannel image segmentation.[8] The image is segmented after a threshold value is selected in any of the color channels. The process is repeated until the histograms for each region become unimodal or the resulting segmentation is sufficient. Forero et al.[9] propose another approach for fuzzy segmentation of color images based on the information that is entailed in each separate chromatic histogram and the proportion of one color channel in relation to another.

A group of fuzzy rules for segmenting images are built from the information of the color images. The first step in developing a set of fuzzy rules to segment an image is to determine the antecedent fuzzy sets. Hence, it is necessary to study the spectral behavior of the images by looking for the conditions that could separate regions in each of the color image channels. In order to build fuzzy rules, the regional conditions which determine the antecedents of the rules of inference, are found via histogram analysis applied to each color component as was seen before in order to establish a particular language rule. Sometimes a channel does not give sufficient information to construct the fuzzy rules and can be ignored. Also, the information obtained from the histograms of each color component is not always enough for segmenting an image. In these cases, the information given by the relationship between the ratio of two channels can make it possible to improve the results.

An image can be considered as an array of fuzzy singletons of size $N \times M$, where each singleton corresponds to an image pixel. Each pixel has a membership value associated with it. To threshold the images, a generalized bell membership function, based on the Cauchy distribution, is used:

$$Q(g;t) = \begin{cases} \frac{1}{1+\frac{|g-m_L(t)|^{2b}}{D}} & \text{if } g \leq t \\ \frac{1}{1+\frac{|g-m_R(t)|^{2b}}{D}} & \text{if } g > t \end{cases} \quad (1)$$

where D is a constant that adjusts the width of the function, $m(t)$ is associated with the center of the class and represents the weighted average of the gray levels and b control the slopes at the crossover point.

The measure of fuzziness is taken as a measure of the uncertainty associated with vagueness of a fuzzy set and is employed to quantify its degree of fuzziness. The measures of fuzziness can be expressed as a function of the gray level histogram and a cost function.[9]

This can be summarized for each measure seen as follows:

- Shannon:

$$S\left[\mu_Q(q,t)\right] = -\mu_Q(q,t)\log_2\mu_1(q,t) - \left[1-\mu_Q(q,t)\right]\log_2\left[1-\mu_Q(q,t)\right] \tag{2}$$

$$f(q,t) = \begin{cases} \sum_{q=0}^{L-1} h(q)S\left[\mu_Q(q,t)\right] & \text{if } 0 < \mu_Q(q,t) < 1 \\ & \text{for } 0 \le t \le L-1 \\ 0 & \text{if } \mu_Q(q,t) = 0 \vee \mu_Q(q,t) = 1 \end{cases} \tag{3}$$

- Kaufmann:

$$K\left[\mu_Q(q,t)\right] = \left|\mu_Q(q,t) - \mu_C(q,t)\right|^d \tag{4}$$

or

$$K\left[\mu_Q(q,t)\right] = \left\{\min\left[\mu_Q(q,t), 1-\mu_Q(q,t)\right]\right\}^d \qquad d \in (0,\infty) \tag{5}$$

$$f(q,t) = \left\{\sum_{q=0}^{L-1} h(q)K\left[\mu_Q(q,t)\right]\right\}^{\frac{1}{d}} \quad \text{for } 0 \le t \le L-1 \tag{6}$$

- Yager:

$$Y\left[\mu_Q(q,t)\right] = 1 - \left|2\mu_Q(q,t) - 1\right|^d \qquad d \in (0,\infty) \tag{7}$$

$$f(q,t) = \left\{\sum_{q=0}^{L-1} h(q)Y\left[\mu_Q(q,t)\right]\right\}^{\frac{1}{d}} \quad \text{for } 0 \le t \le L-1 \tag{8}$$

- Gauss:

$$G\left[\mu_Q(q,t)\right] = \begin{cases} e^{-\frac{1}{2}\left[\frac{\mu_Q(q,t)-c}{\sigma}\right]^2} & \text{if } 0 < \mu_Q(q,t) < 1 \\ 0 & \text{if } \mu_Q(q,t) = 0 \vee \mu_Q(q,t) = 1 \end{cases} \tag{9}$$

$$f(q,t) = \sum_{q=0}^{L-1} h(q)G\left[\mu_Q(q,t)\right] \quad \text{for } 0 \le t \le L-1 \tag{10}$$

The concept of the measure of fuzziness associated to the histogram is used for the optimal selection of the threshold in order to binarize the image. The fuzziness function $f(q,t)$ is calculated for all the values of t. The optimal threshold t^* is the one that minimizes $f(q,t)$:

$$t^* = \arg\left[\min f(q,T)\right] \qquad 0 \le t \le L-1 \tag{11}$$

or better,

$$t^* = \arg\left[\min f(q,T)\right] \qquad q_{min} \le t \le q_{max} \tag{12}$$

a

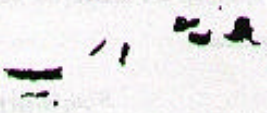

b

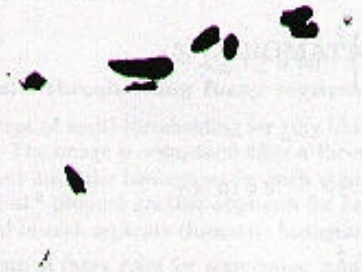

c

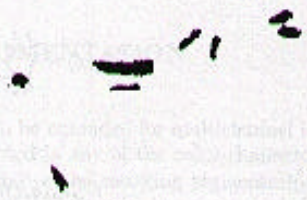

d

Figure 1. (a) Original image;(b) Red channel. Yager $b = 0.731$; (c) Green channel. Yager $b = 0.184$; (d)Blue chan
Yager $b = 0.875$, $d = 3.000$

The optimal threshold t^* is then defined as the level that maximizes as much as possible the separat
between the two class means, that is when the fuzziness is minimal.

The above mentioned color technique was tested on an database of 30 "bacilli" images. An example of
image is shown in Fig. 1. The best results are given by the Yager method with d=0.875 and Cauchy w
b=3.0.

3.2. Color separation

It is well known that segmentation using color provides a broader discrimination between object borders.[10]
consider here a simple color filtering account by calculating the ratio of the inverse of the yellowish stai
bacteria (blue channel) with the product of the other two chromatic channels (see Eq.13).

$$C = \frac{B}{R * G + \epsilon} \qquad (1$$

where R,G,B represent the red,green and blue channels and inverse of C represents the percentage of the yell
color in the images in comparison with the other two chromatic channels. The value ϵ in the denominator

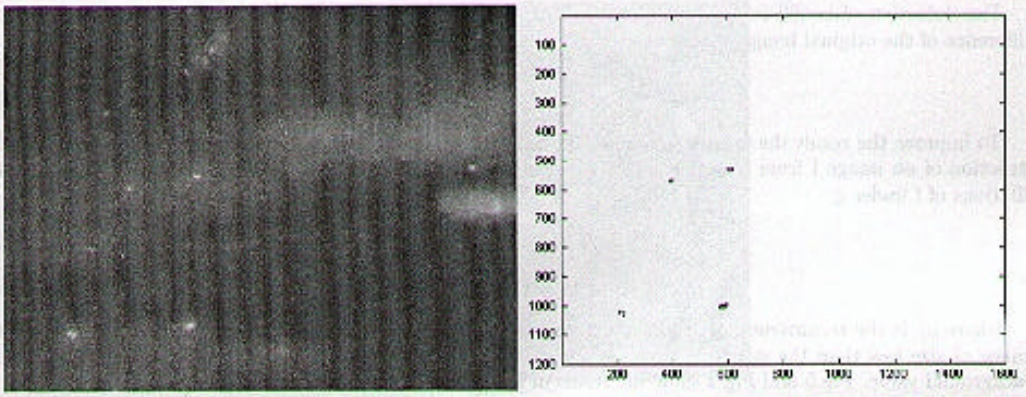

Figure 2. a Original image.b Its yellow region segregation

Eq. 13 can be taken as a small constant to avoid the division by zero, or simply ignoring such points. Fig. 2 shows and example of a positive tuberculosis image (left) and the corresponding result of Eq.13 (right). We have empirically observed the presence of yellowish and greenish structures for a $C > 0.7$. For values $C > 0.7$ it is necessary to combine the simple detection by color with a shape detector in order to reject i.e. the large string-shaped cultured regions that are not of interest in this study. Besides that, we have accomplished a specificity study with 100 negative images provided by expert clinicians. Specificity is the ratio of true negative decisions to the total number of negatives). High values of specificity have been achieved for the test set (91% specificity for the greenish regions and 99% specificity for the yellowish regions).

4. MORPHOLOGICAL IMAGE SEGMENTATION

In the area of phase-contrast microscopy, Liu et al have proposed a computer-aided interactive system for analyzing the morphological diversity of microbial communities.[11] The system called CMEIAS consists of several custom plugins for use with UTHSCSA ImageTool software.[12]
We have evaluated a segmentation scheme for bacilli detection based on mathematical morphology operations. Mathematical morphology[13] is an image processing approach based on set-theoretical operations. It was first designed for binary images and extended to grayscale data.[14] The basic grayscale morphological operations are dilation and erosion, which can be defined as follows. Given two functions $f : F \to E, k : K \to E$, dilation $f : F \oplus K \to E$ can be obtained as:

$$(f \oplus k)(x) = max f(x - z + k(z) \; z \in K, x - z \in F \tag{14}$$

where K is referred to as structuring element.
On the other side, erosion $f \ominus k : F \ominus K \to E$ can be defined as:

$$(f \ominus k)(x) = min f(x + z) - k(z) | z \in K \tag{15}$$

The combination of both operations results in the operation called opening $f \circ k$:

$$(f \circ k) = (f \ominus k) \oplus k \tag{16}$$

The detection of bacilli in the image was obtained using a top-hat operation[13] which is the result of the difference of the original image an and opened version of it:

$$TopHat(I) = I - (I \circ k) \tag{17}$$

To improve the result the opened image was reconstructed[15] before applying the top-hat. Grayscale reconstruction of an image I from a second image J, such that $J < I$ is the result until convergence of successive dilations of f under g:

$$\rho_I^{(0)}(J) = J \tag{18}$$

$$\rho_I^{(n)}(J)(p) = min(I(p), (\rho_I^{n-1}(J) \oplus k)(p)) \tag{19}$$

where ρ_I^J is the reconstruction of image I from image J. The top-hat allows to extract peaks of grey of an image of size less than the structuring element used. The result of the operation is independent of the local background value. Fig.3 and Fig.4 show the result of applying the top-hat to an image of bacilli.

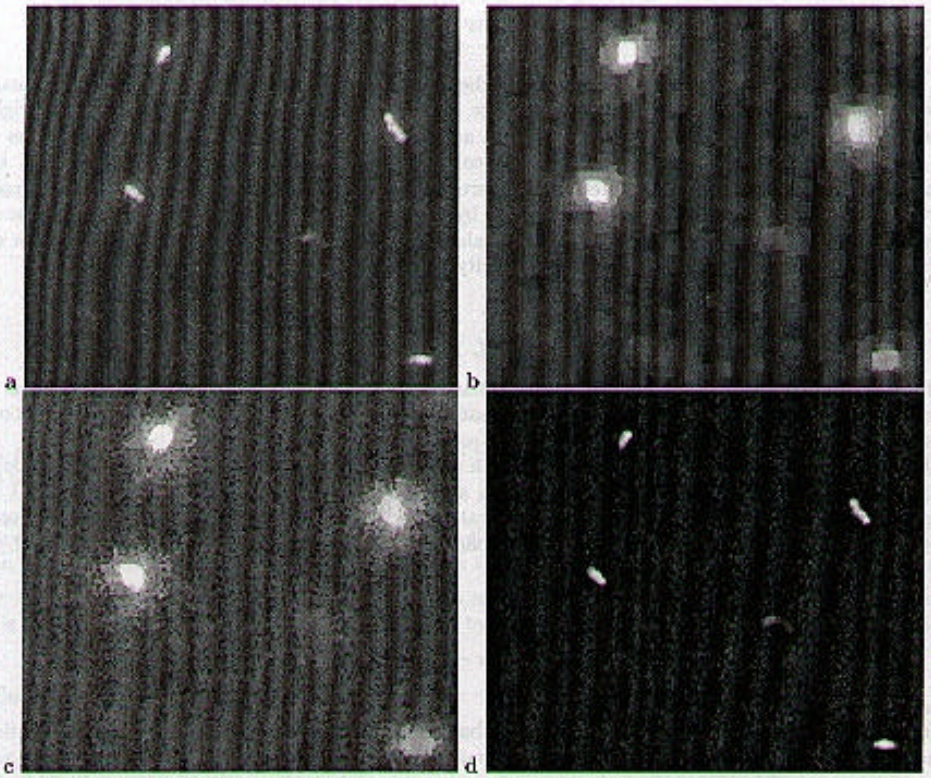

Figure 3. (a) Original image.(b) Result of opening. (c) Reconstructed image. (d) Top Hat

The images are thresholded to obtain a binary image. The threshold was set at value of 30, obtained by evaluating different values in a training set of images.

Figure 4. Final image with contours object contours superimposed

To classify objects, several parameters of each object were obtained using ImageTool,[12] namely area, perimeter, major and minor axis lengths and angles, elongation, roundness, minimum gray-level, maximum gray-level, gray level density. Three object classes were defined to classify the objects, namely, bacilli, possible bacilli and debris. A training set consisting of 80 images with bacilli and 50 *negative* images (known to contain no bacilli) was used. The most discriminant features were selected using a stepwise input / output F-test to add and to remove variables.[16] The most discriminant features are area, graylevel density (i.e. mean gray level of the object), major axis length (i.e. length of the longest line that can be drawn through the object) and circularity (i.e. $4\pi * area/(perimeter)^2$). Based on this, a Fisher linear discriminant was designed to classify the objects. An initial classification with a limited set of cultures produced 82% of specificity. Further extensive clinical evaluation research is required to improve such results, especially in the case of cultures with contain a lot of debris.

5. SIGNATURE EXTRACTION

In this section we describe an image identification method based on the use of the so-called *signatures*. The term signature is given since this kind of representations are non-invertible. The detection of image or pattern changes invariant onto geometric transformations are required in many applications. If we translate an image, all the shifting information appears in the phase of the Fourier transform. Similarly, if we scale or rotate an image all the information about the amount of scaling or rotation appears in the phase of the scale transform. The scale transform provides us a transform that is insensitive to scaling or rotation. In this way, we use the scale transform properties for image identification. The scale transform was defined by [17] for 1-D signals and extended by[18] for 2-D images. The extraction of image signatures has been the subject of interest of many authors. An invariance signature is a measure of the degree to which the image (or a particular image feature) is invariant under a variety of transformations. Fares et al.[19] have proposed to recognize rotated patterns by extracting signatures from the Fourier phase. Milanese and Cherbuliez[20] proposed a method for computing an image signature by projecting logarithmic-polar mappings onto 1D vectors for image retrieval. This representation provides a very compact description of all image aspects, including shape, texture and color. We propose here to extend the Cherbuliez and Milanese method to facilitate the image identification process. The main advantage of using signatures is the dramatic reduction of image dimensionality and also facilitates indexing.[20] The signature method is based on the computation of vector projections of a scale-based or Fourier-Mellin representation. Fig. 2 shows and example of the method. Fig. 2a shows the input image. Fig. 2b shows the log-polar mapping of the power spectrum of the input image. Fig. 2c-d shows the projection of the log-polar map along the horizontal an vertical directions (i.e. the marginals). Then, if we compute the power

spectrum of such projections we will have a representation invariant to rigid transformations (i.e. translation, rotation and scale). It is important to remark that the signature vectors provide a compact representation of a gray level image. In the case of the tuberculosis images, we can consider only the green channel or to consider three different pairs of vectors corresponding to each color channel. Once extracted the signatures we can use a simple Euclidean distance function between signatures in order to evaluate a similarity measure. Future work will require to compute an image database of ground-truth signatures to provide a quantitative measure of the identification process.

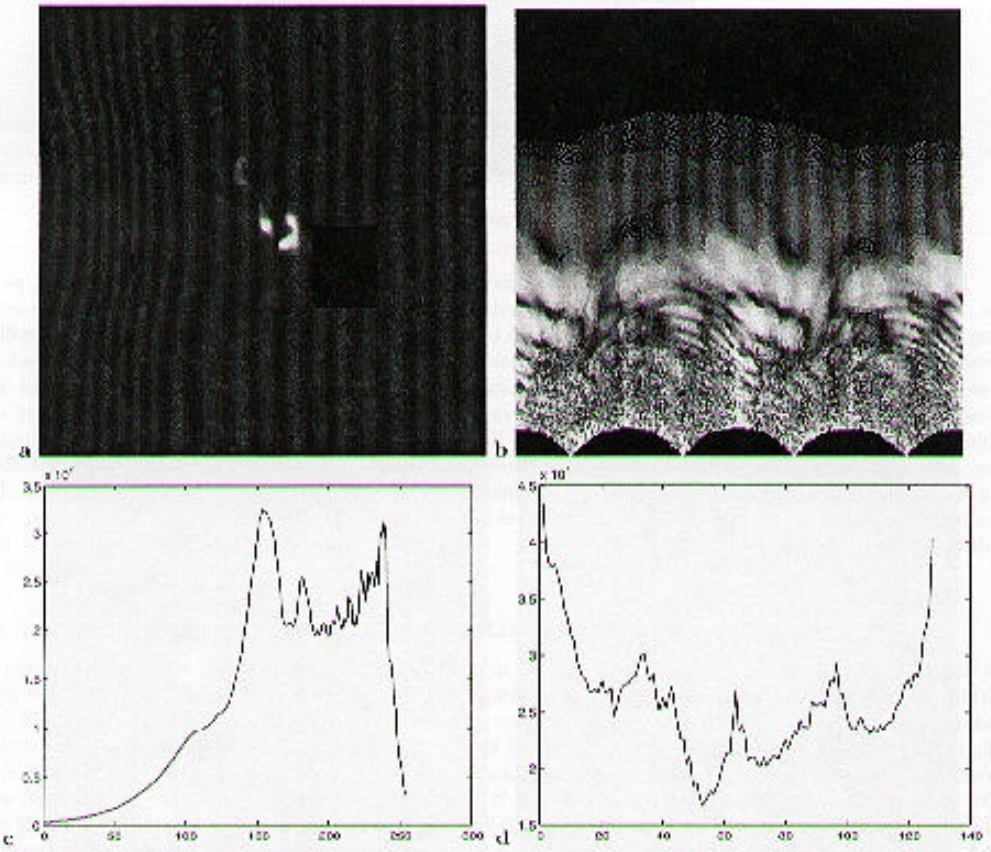

Figure 5. (a) Original image.(b) Log polar mapping (c) Radial projection (d) Angular projection

6. AUTOFOCUS ALGORITHMS FOR TUBERCULOSIS IMAGES

The automation of fluorescence stained mycobacteria first require a reliable, accurate and fast autofocus measure. Many autofocus algorithms have been proposed in the literature. Elsewhere we have evaluated and compared an extensive number of autofocusing methods in cytogenetic studies. For such kind of images we concluded that functions based on correlation measures provides the best autofocus performance. For fluorescence stained mycobacteria we performed a preliminar study testing a stack of 25 images from the same object taken at various distances from the focus point. All the autofocus measures have been extracted considering only the green channel that appears to be more discriminant for this type of images. If we compute the logaritdm of

the histogram from each image, we can observe that for heavily defocus image the variance of such histogram is smaller than for slightly defocus or in-focus images.

The automatic evaluation of focus is a challenging task, which requires a reliable, accurate and fast autofocus procedure. 25 images of one blood sample acquired at different focus distances were used as the input to our focus assessment procedure. We refer to the images as image 1 to image 25, where the correct focus was reached for images around 16 and decreases in both directions towards image 1 and 25. The objects of our study (tuberculosis bacteria) occupy only a small part of the image and this proved to be a serious obstacle for standard focus measures. For comparison, we applied four standard techniques. The most simple focus measure was grey level variance of an image[21]

$$M_{var} = \sum_i \sum_j (g(i,j) - \bar{g})^2 \ , \tag{20}$$

where g is the image grey level function and $\bar{g}$ denotes the mean value of g. The second was the energy of image Laplacian

$$M_L = \sum_i \sum_j g(i-1,j) + g(i+1,j) + g(i,j-1) - g(i,j+1) - 4g(i,j) \ , \tag{21}$$

which is, according to Subbarao,[22] more robust to noise than the image variance or gradient energy. The third was a very recent wavelet-based measure (M_{wb}) proposed in,[23] which calculates the energy ration between a low-pass band and several high-pass bands. The last focus measure, which we used, was based on autocorrelation function[24] and defined as

$$M_{cor} = \sum_i \sum_j g(i,j)g(i+1,j) - \sum_i \sum_j g(i,j)g(i-2,j) \ . \tag{22}$$

This measure was found to be the most appropriate for cytometry studies[21] that were conducted on images similar to ours. Although each of the above measures were successfully applied to different sorts of images, none of them produced meaningful results in our case when applied to the whole images, see Fig. 6. The important contribution of tiny bacteria to the overall measure is negligible small compare to the contribution of the irrelevant noisy background. When only a small rectangular neighborhood (256×256) containing a bacterium was considered, M_{wb} and M_{cor} were able to localize the focused image, see Fig. 6. However, this procedure is not fully automatic, since the positions of bacteria are not known in advance and must be be manually determined.

We were thus forced to propose a novel focus measure based on image histogram that works on the whole image. It is generally true that focused images have a greater number of grey levels than unfocused images. Likewise, the image histogram can be considered as a probability distribution function (pdf) and then variance of pdf increases as the image focus increases. Since the tiny bacteria are much lighter than the background, they contribute solely to the upper part of the histogram. To avoid the above mentioned problem of the insufficient contribution, we take the logarithm of histogram. Our proposed variance of log-histogram thus takes the form:

$$M_{log} = \sum_k (k - E\{p\})^2 \log(p_k) \ , \tag{23}$$

where p_k is the relative frequency of grey level k and $E\{p\} = \sum_k k \log(p_k)$ is the expected value of log-histogram. Fig. 6-8 show three image examples from a heavily defocus image (Fig. 6) to the image on focus (Fig. 8). The obtained results included in Fig. 9 illustrate that this focus measure can be used for a fast and fully automatic evaluation of focus. Apart from the slight shift of the global maximum, the proposed focus measure behaves correctly, and in comparison with the other measures it is relatively smooth.

ACKNOWLEDGMENTS

This research is supported in part by the EU MAST3 ADIAC project and the III-PRICYT of the Comunidad de Madrid. The authors acknowledge the financial help of a co-operative programme: CSIC (Spain) - CONACYT (México) and the CONACYT project 36075-B. We thank to J.L. Pech-Pacheco for digitizing the tuberculosis images at the Hospital Gregorio Marañon in Madrid (Spain).

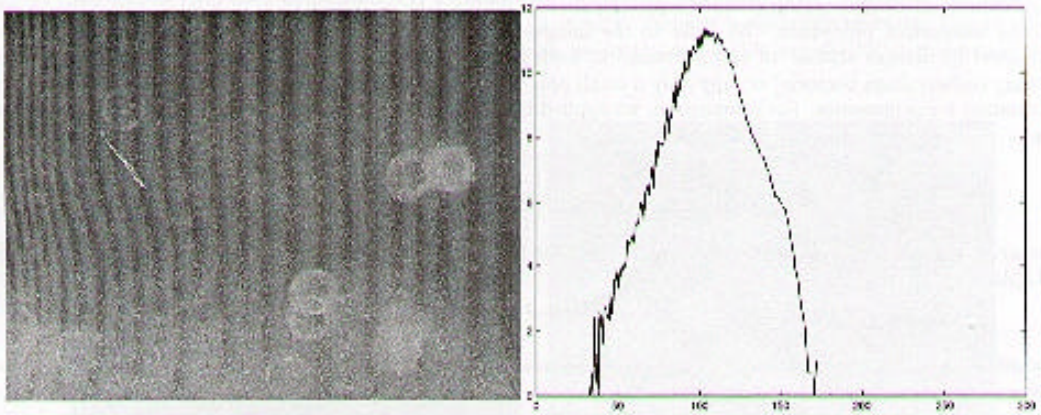

Figure 6. (a)Image no. 1 - heavily defocus image. (b) Its histogram.

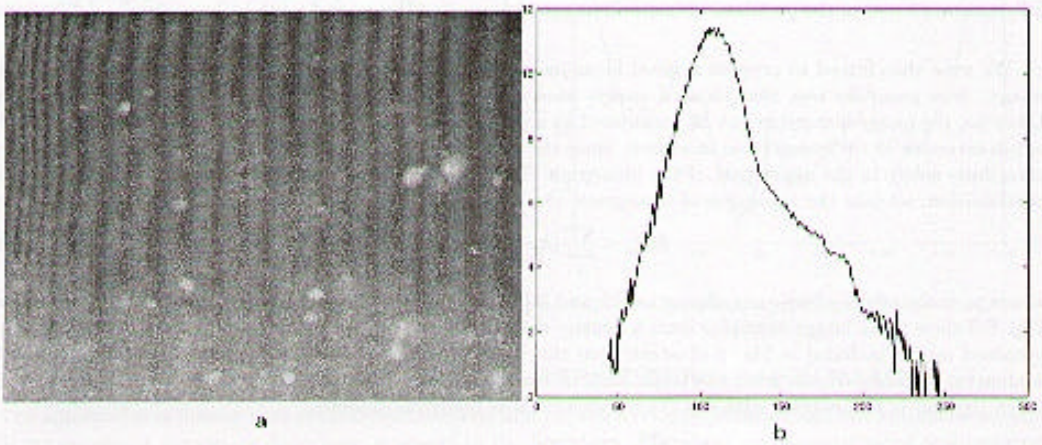

Figure 7. (a) Image no. 10 - slightly defocused image. (b) Its histogram.

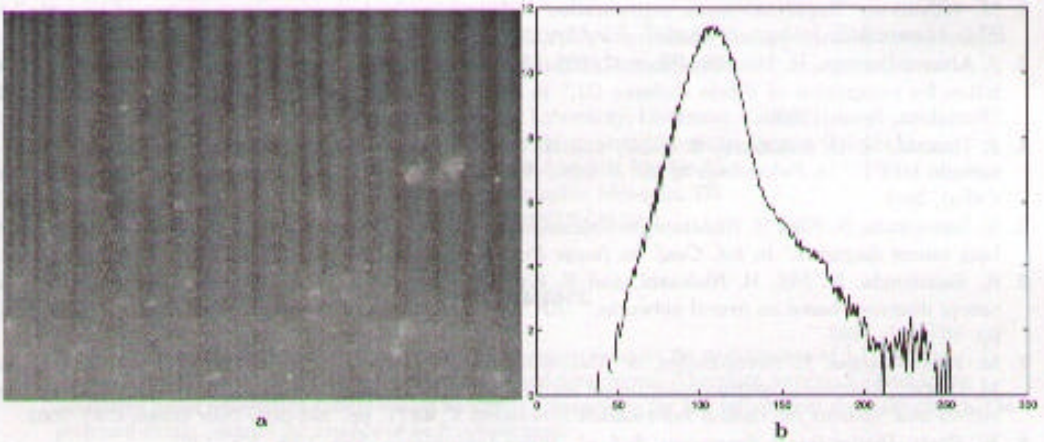

a b

Figure 8. (a) Image no. 15 - image in focus.(b) Its histogram.

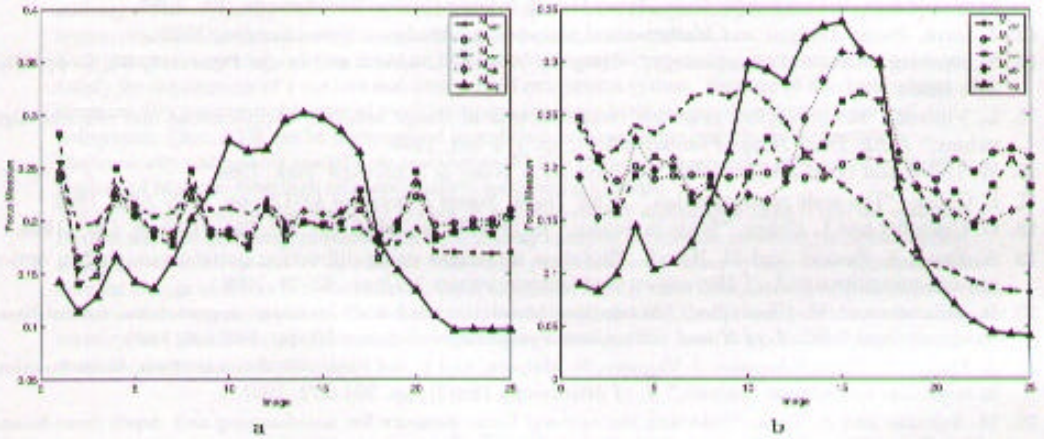

a b

Figure 9. (a) Focus measures calculated on the whole images 1 to 25. (b) Focus measures calculated on the 256×256 rectangular section of the images 1 to 25 containing a tuberculosis bacterium. The plotted values are normalized.

REFERENCES

1. K. Veropoulos, G. Learmonth, B. Knight, and J. Simpson, "Automated identification of tubercle bacilli in sputum," *Anal. and Quantitative Cytology and Histology* **21**(4), pp. 277–281, 1999.
2. M. Wilkinson, "Rapid automatic segmentation of fluorescent and phase-contrast images of bacteria," in *Fluorescence Microscopy and Fluorescent Probes*, J. Slavik, ed., Plenum Press, New York, NY, 1996.
3. J. Alvarez-Borrego, R. Mouriño Pérez, G. Cristobal, and J. Pech-Pacheco, "Invariant optical color correlation for recognition of Vibrio cholerae O1," in *Int. Conf. on Pattern Recognition*, **2847**, pp. 283–286, (Barcelona, Spain), 2000.
4. P. Demantova, D. Sakamoto, S. Ioshii, and H. Gamba, "Segmentacao automática de bactérias para o método DEFT," in *Proceedings of the II Latin American Congress on Biomedical Engineering*, (Havana, Cuba), 2001.
5. R. Sammouda, N. Niki, H. Nishitani, S. Nakamura, and S. Mori, "Segmentation of sputum color image for lung cancer diagnosis," in *Int. Conf. on Image Processing*, 1, pp. 243–246, (Washington D.C.), 1997.
6. R. Sammouda, N. Niji, H. Nishitani, and E. Kyokage, "Segmentation of sputum color image for lung cancer diagnosis based on neural networks," *IEICE Transactions on Information and Systems* **E-81-D**(8), pp. 862–871, 1998.
7. M. Forero-Vargas, F. Sierra-Ballen, J. Alvarez-Borrego, J. Pech-Pacheco, G. Cristobal, L. Alcala, and M. Desco, "Automatic sputum color image segmentation for tuberculosis diagnosis," in *SPIE Proc. Algorithms and Systems for Optical Information Processing V*, **4471**, pp. 293–304, (San Diego, CA), 2001.
8. W. Pratt, *Digital Image Processing, 2nd. ed.*, Wiley-Interscience, New York, NY, 1991.
9. M. Forero, "Fuzzy thresholding and histogram analysis," in *Fuzzy filters for image processing. Series Studies in Fuzziness and Soft Computing*, M. Nachtegael, D. V. der Weken, D. V. D. Ville, and E. Kerre, eds., Springer Verlang, 2002.
10. J. Geusebroek, *Color and geometrical structure in images. Applications in microscopy*. PhD thesis, Universiteit van Amsterdam, 2000.
11. J.Liu, F. Dazzo, O. Glagoleva, B.Yu, and A. Jain, "CMEIAS: A computer-aided system for the image analysis of bacterial morphotypes in microbial communities," *Microbial Ecology* **41**, pp. 173–194, 2001.
12. C. Wilcox, S. Dove, W. Doss-McDavid, and D. Greer, "UTHSCSA ImageTool." `http://ddsdx.uthscsa.edu`, Univ. Texas Health Science Center, San Antonio, TX, 1997.
13. J. Serra, *Image Analysis and Mathematical Morphology*, Academic Press, London, 1982.
14. S. Stenberg, "Grayscale morphology," *Computer Vision, Graphics and Image Processing* **35**(3), pp. 335–355, 1986.
15. L. Vincent, "Morphological grayscale reconstruction in image analysis: Applications and efficient algorithms," *IEEE Trans Image Processing* **2**(2), pp. 176–201, 1993.
16. W. Dillon and G. M., *Multivariate Analysis*, John Wiley & Sons, New York, 1984.
17. L. Cohen, "The scale representation," *IEEE Trans. Signal Processing* **41**(12), pp. 3275–3292, 1993.
18. G. Cristobal and L. Cohen, "Scale in images," in *SPIE Proc.*, **2846**, pp. 251–261, (Denver, CO), 1996.
19. A. Fares, A. Bouzid, and M. Hamdi, "Rotation invariance using diffraction pattern sampling in optical pattern recognition," *J. of Microwaves and Optoelectronics* **2**(2), pp. 33–39, 2000.
20. R. Milanese and M. Cherbuliez, "A rotation, translation and scale-invariant approach to content-based image retrieval," *Int. J. of Visual Comm. and Image Representation* 10, pp. 186–196, 1999.
21. A. Santos, C. Ortiz-Solorzano, J. Vaquero, N. Malpica, and F. del Pozo, "Evaluation of autofocus functions in molecular cytogenetic analysis," *J. of Microscopy* **188**(3), pp. 264–272, 1997.
22. M. Subarao and J. Tyan, "Selecting the optimal focus measure for autofocusing and depth-from-focus," *IEEE Trans. Pattern Analysis and Machine Intelligence* **20**, pp. 864–870, 1998.
23. J. Kautsky, J. Flusser, B. Zitová, and S. Šimberová, "A new wavelet-based measure of image focus," *Patt. Recog. Letters* , in print, to appear in 2002.
24. D. Vollath, "Automatic focusing by autocorrelative methods," *J. Microsc.* **147**, pp. 279–288, 1987.